IOPscience iopscience.iop.org

Home Search Collections Journals About Contact us My IOPscience

Multiple atomic scale solid surface interconnects for atom circuits and molecule logic gates

This article has been downloaded from IOPscience. Please scroll down to see the full text article.

2010 J. Phys.: Condens. Matter 22 084025

(http://iopscience.iop.org/0953-8984/22/8/084025)

View the table of contents for this issue, or go to the journal homepage for more

Download details:
IP Address: 129.252.86.83
The article was downloaded on 30/05/2010 at 07:19

Please note that terms and conditions apply.

J. Phys.: Condens. Matter **22** (2010) 084025 (18pp) doi:10.1088/0953-8984/22/8/084025

Multiple atomic scale solid surface interconnects for atom circuits and molecule logic gates

C Joachim[1,2], D Martrou[1], M Rezeq[2], C Troadec[2], Deng Jie[2], N Chandrasekhar[2] and S Gauthier[1]

[1] Centre d'Elaboration de Matériaux et d'Etudes Structurales (CEMES-CNRS) 29, rue Jeanne Marvig, BP 94347, 31055 Toulouse Cedex 4, France
[2] Institute of Materials Research and Engineering, A*STAR (Agency for Science, Technology and Research), 3 Research Link, 117602, Singapore

Received 5 June 2009, in final form 12 September 2009
Published 5 February 2010
Online at stacks.iop.org/JPhysCM/22/084025

Abstract
The scientific and technical challenges involved in building the planar electrical connection of an atomic scale circuit to N electrodes ($N > 2$) are discussed. The practical, laboratory scale approach explored today to assemble a multi-access atomic scale precision interconnection machine is presented. Depending on the surface electronic properties of the targeted substrates, two types of machines are considered: on moderate surface band gap materials, scanning tunneling microscopy can be combined with scanning electron microscopy to provide an efficient navigation system, while on wide surface band gap materials, atomic force microscopy can be used in conjunction with optical microscopy. The size of the planar part of the circuit should be minimized on moderate band gap surfaces to avoid current leakage, while this requirement does not apply to wide band gap surfaces. These constraints impose different methods of connection, which are thoroughly discussed, in particular regarding the recent progress in single atom and molecule manipulations on a surface.

(Some figures in this article are in colour only in the electronic version)

1. Introduction

Single molecule mechanics [1], mono-molecular electronics [2] and multi-probe experiments on atomic scale constructed devices [3] or machinery (memory, transducers) [4] require the development of a specific surface interconnection technology able to provide a large number of information and energy access channels to the atomic (or molecular) scale machinery constructed on a surface (see figure 1) with atomic precision and cleanliness [5]. Atomic precision is compulsory for all these devices and machinery because when the end of a molecule electronically interacts with its metallic interconnection pads, an optimum contact conductance is obtained for inter-atomic distances between the 0.2 nm chemisorption and the 0.3 nm van der Waals distance ranges. For a conjugated molecular wire connected to copper electrodes, the optimum was demonstrated to be around 0.25 nm [6]. A 0.2 nm adsorption distance would lead to a strong electronic coupling between the molecule π system and the pads, changing the pad metallic density of state locally. This change increases the reflection coefficient of the metallic Bloch waves on the pad–molecule–pad junction and therefore decreases its conductance [6]. An adsorption distance above 0.3 nm would be too large for an overlap between the π electronic system of the molecule and the pad yet large enough to lead to efficient electron transfer events. The required 0.05 nm precision in distance implies a perfect control of each atom position on the pads and of the atomic composition of the corresponding contact surface where the molecular electronic cloud will overlap with the metallic pads. Therefore, atom control and atomic precision are the keys to success for perfectly reproducible experiments on a single molecule for devices or machine applications, as illustrated in figure 1. Mastering such a precision will avoid the statistical approach that is commonly used, for example in molecular wire conductance measurements on ill-defined systems [7].

 © 2010 IOP Publishing Ltd Printed in the UK

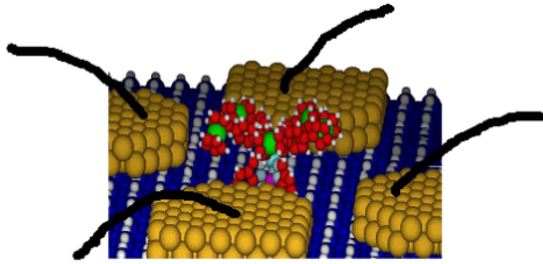

Figure 1. A single five wings molecule motor [1] positioned between a 4 Au nanopad junction constructed on a Si(100)-H surface. The motor is driven by the tunneling electrons sequentially transferred through the motor wings. The 4 black wires coming out of the surface are indicative of the interconnection step 3, discussed in the text, depending on the electronic gap of the supporting surface.

At the end of the 1980s, it was expected that e-beam nanolithography would be able to provide such an interconnection technology [8]. But with its resist based approach (be it a grown, a deposited or a contamination resist), e-beam nanolithography can not make it in a planar approach [9], because it is not able to respect simultaneously the atomic scale precision, cleanliness and the expected large number, N, of access channels to the atomic or molecular scale machinery [10]. Alternative new surface nanolithography techniques, such as nano-imprint [11] or nanostencil [12], are neither adapted to encompass all the interconnection stages from the macroscopic to the atomic scale, nor clean enough down to the atomic scale. At the turn of the century, this problem associated with new targets in atomic scale machinery such as molecule logic gates [13], molecule motors [1] and surface atomic scale electronic circuits [14] triggered a new approach starting from the bottom; that is from the fundamentals of surface science.

This review describes the new laboratory scale approaches explored today to solve this multi-access atomic scale precision interconnection problem for electrical interconnects. The same question can be put forward for photonic multi-access to the atomic scale in a planar approach [15]. In section 2, the general principles of the few UHV interconnection machines in construction are described. We distinguish 2 types of machines, depending on the electronic gap of the surface, where the atomic scale devices and machinery are supposed to run. Section 3 describes an atomic scale interconnection machine devoted to wide gap semiconductor and insulator materials. Section 4 describes a machine devoted to moderate gap semiconductor surfaces. In each case, the surface science problems experimented, solved or yet to be solved are described. In conclusion, we discuss the large N limit of this atomic scale interconnection approach with electrons and how to pass from laboratory scale UHV interconnection machines to a more industrial-like approach. The work reported here is one output of the EU ICT integrated project Pico-Inside in Toulouse and of the VIP A*STAR Atom Tech program in Singapore.

2. Atomically precise electrical interconnection machine

An atomic scale precision multiple access interconnection machine must provide N conducting wires converging toward a very small surface area where an active machine (see figure 1 for a $N = 4$ example) has been constructed or assembled with atomic scale precision. These N interconnects are positioned somewhere on a large handleable wafer surface. As a consequence, a very efficient navigation system must be designed to locate this very small active area from a macroscopic perspective while keeping the local atomic precision of the interconnection construction. The solution to this navigation requirement is to combine two types of microscopy: a far field one (optical microscopy, scanning electron microscopy (SEM)) for large scale navigation and a near field one (scanning tunneling microscopy (STM), atomic force microscopy (AFM)) for the atomic scale part, with a compulsory overlap between these 2 types of microscopy.

In air, the combination of an optical microscope with a standard AFM to interconnect a single wall carbon nanotube on metallic nanoelectrodes made by e-beam nanolithography has already shown the power of this combination of two microscopes, associated with a dedicated way to electrically contact the nanopads [16]. The contacts were taken by introducing, under the AFM head, a comb of metallic microcantilever electrodes to minimize the overall length of the electrical circuit fabricated on the wafer surface [16]. While not atomic scale, this proof of concept demonstrates all the ingredients that are at the basis of the next generation UHV and atomic scale interconnection machines, as schematically presented in figure 2.

A UHV atomic scale interconnection machine is designed to follow *a dedicated interconnection sequence*. On an atomically clean well-prepared surface, an *atomic scale circuitry* is fabricated (A). This circuit must have a minimal lateral extension to make possible its connection to a large number N of *metallic nanopads* (B) positioned around it. In the example of figure 2, a molecule is connected to these nanopads by *atomic metallic wires*. Depending on the electronic surface gap of the supporting material, the nanopads (B) have to be contacted from the top by a series of N atomically sharp *metallic tips* (C1) or by a series of N *nanoscale wires* (C2) up to the point where mesoscopic metallic wiring or *microelectrodes* (D) can be surface fabricated and contacted by N *microscale metallic cantilevers (E)* also from the top of the wafer. What determines the choice of the interconnection technology between C1 and C2 (and after the need for the D and E interconnection steps in figure 2(b)) is the electronic gap of the surface, which in turn dictates the kind of far field microscopy to be used for navigation over the wafer surface.

For a large valence band–conduction band (VB–CB) electronic surface gap (more than a few eV up to 12 eV for good insulators), SEM is difficult to use because the electron beam will charge the surface. In this case, an optical microscope must be used. This microscope determines the minimum length of metallic surface wiring that must be

Table 1. Some of the most studied wide band gap semiconductors and insulators.

Material	KBr	MgO	Al_2O_3	CaF_2	4H-SiC	2H-GaN	2H-AlN
Bulk band gap (eV)	6.6 [88]	7.8 [89]	8 [90]	12.1 [91]	3.07 [92]	3.47 [92]	6.28 [92]

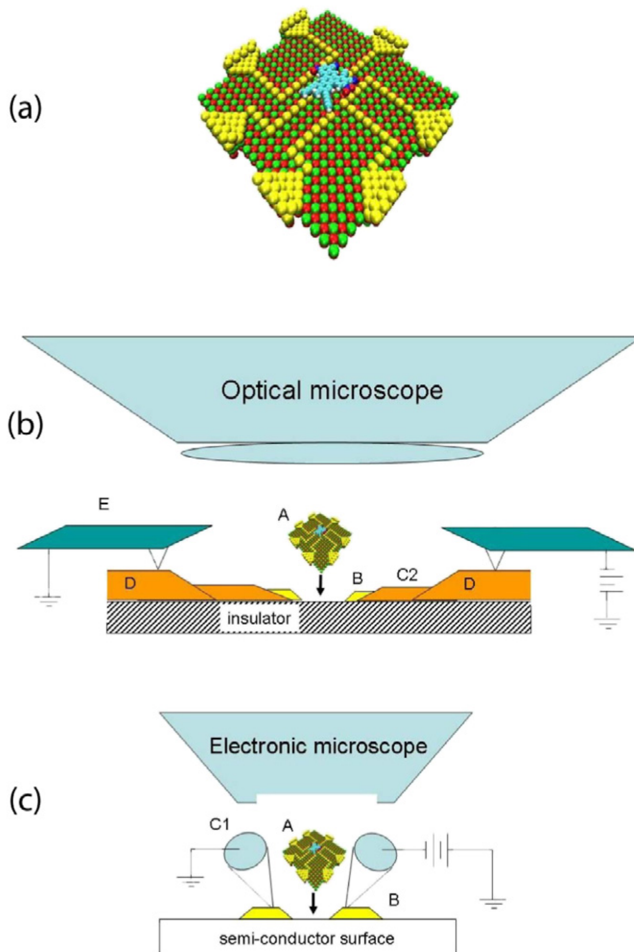

Figure 2. Scheme of the atomic scale interconnection machines for (b) wide and (c) moderate surface band gap substrates. (a) and A: the atomic scale circuitry embedded into the surface, B: contacting metallic nanopads, C1: ultra-sharp metallic tips, C2: nanowires, D: microelectrodes, E: metallic microcantilevers.

fabricated starting from the nanopads (B) toward the next contact stage based on metallic microcantilevers (figure 2(b)). Fortunately, with a large surface gap, the surface area of those interconnects can be expanded laterally without significant leakage currents between the different electrodes. This is the basis of the UHV interconnection machine described in section 3 where a low temperature approach is not compulsory.

For a moderate VB–CB electronic surface gap (around a few eV), it is not possible to use very long surface metallic circuitry due to the leakage currents that will appear between the surface electrodes. In this case, one solution is to use ultra-sharp STM-like tips positioned from the top on the nanopads (figure 2(c)). In this case, the bulk of the tip is not in contact with the supporting surface and one goes continuously from the tip apex radius of curvature of a few nanometer up to the 100 μm or more of a section of the tip body. In this case, navigation on the surface can be performed using an UHV-SEM (figure 2(c)) by grounding the sample during SEM imaging to avoid charging. This is the basis of the UHV interconnection machine described in section 4. Here, a low temperature approach is compulsory to limit leakage currents due to the low electronic gap of the surface of the supporting material.

3. Large electronic surface gap supporting materials

As presented in figure 2(b), a large surface electronic gap for the material supporting the interconnection structure leads to 5 levels of interconnects. Levels (A) and (B) depend on our mastering of atomic scale surface science phenomena while level (C), (D) and (E) rely on mesoscopic scale surface phenomena such as surface wetting, associated with developments in UHV instrumentation. The starting point of a multi-access interconnection technology on a large electronic gap surface material is the careful selection and surface preparation of the supporting material. In this section, the progress and the problems that remain to be solved for these 5 levels are presented up to the description of the interconnection machine developed in Toulouse.

3.1. Atomic scale circuitry (level A)

3.1.1. Surface selection and preparation. For natural as well as for artificial mineral crystalline compounds, a wide band gap is more the rule than the exception. But, in this huge class of materials, only a few have been investigated in detail by surface science techniques, mainly because of the inadequacy of techniques using electron beams to study them. Stringent conditions should be satisfied to make possible the construction of the first atomic scale level (A) of the interconnection sequence presented in figure 2(b): the surface should be (1) atomically clean, with a well-controlled stoichiometry, (2) atomically flat, with large enough terraces and (3) should present few defects. In these conditions, a typical 50 nm $\times$ 50 nm 'perfect' area, suitable to accommodate the atomic scale device, becomes readily accessible. A selection of wide band gap materials that have been studied in detail, either for their simplicity or for their applications, and that satisfy these requirements, is presented in table 1.

KBr is representative of the family of alkali halides, the archetype of ionic compounds. The most stable surface, prepared by cleavage, is the non-polar (001) surface. Large atomically clean terraces are easily obtained. MgO is one of the simpler ionic oxides, used for instance as a model catalyst. Cleavage allows a clean surface to be obtained with the nominal stoichiometry of the material. The surfaces of the different phases of alumina have been studied for a

long time, but despite their technological interest, their atomic structure remains largely unknown. They are difficult to prepare and usually present complex phase diagrams, where the surface stoichiometry plays a determining role. CaF_2 is an ionic insulator that has been considered for a long time as a good candidate for an insulating material in microelectronics due to its small lattice mismatch with Si. It is nowadays investigated for its optical properties for the fabrication of lenses for deep UV optical lithography. The $CaF_2(111)$ surface can be obtained by cleavage. It is atomically flat over large areas. SiC is one of the most studied wide band gap material, finding applications in such diverse area as power electronics, microelectromechanical systems and as a supporting material for graphene. It exists in different polytypes, which display a rich variety of surface reconstruction, some of which have been investigated in detail by STM [17]. More recently, group-III nitride semiconductors (GaN, AlN) have attracted much interest for their applications as short wavelength optical emitters and detectors, as well as for high-speed electronics. A large variety of surface structures is obtained depending on the growth method and conditions. Some of these surfaces have been studied in detail, in particular by STM [18].

For all these materials, the *surface* band gap should be distinguished from the *bulk* band gap: for instance, at the MgO(001) surface, the band gap is reduced from the bulk value of 7.8 eV to 6.2 eV, due to an unoccupied surface state [19]. An extreme case is that of the metal-rich termination of GaN(0001) and AlN(00001) faces, which is metallic [18].

Some of these materials have also been studied in the form of ultra-thin insulating layers adsorbed on a conductive substrate, in particular by STM. (For a recent review, see [20].) Useful information can be extracted from these studies, but caution should be exercised because they cannot always be extrapolated to the thicker films that are needed for building the interconnection described here to limit the leakage current between the interconnection pads.

3.1.2. Atomic scale imaging: NC-AFM. After the surface preparation, STM atomic scale surface imaging is practical only for SiC, GaN, and the metal-rich faces of AlN, among the compounds listed in table 1. Fortunately, recent progress in AFM imaging with the so-called non-contact (NC) or frequency modulation (FM) mode [21, 22] has opened the way to atomic and molecular resolution on large gap and insulating surfaces. Notice that this NC-AFM can be efficiently combined with optical microscopy if suitable markers in the micron range are fabricated on the substrate, as discussed at this end of this section.

In NC-AFM, the cantilever is embedded in a positive feedback loop that oscillates at the cantilever resonance frequency while another loop maintains its oscillation amplitude at a pre-set value. In contrast to the amplitude modulation (AM) or 'tapping' [23] method, where the frequency is externally fixed, the resonance frequency of the cantilever in the FM method varies under the influence of the tip–sample forces. A 'topographic' image is obtained by scanning the surface while adjusting the tip–substrate distance required to maintain this frequency shift at a pre-set value. The specificity of this method is that very high quality factors force sensors, which lead to increased force sensitivity, can be used without penalizing the acquisition time, as in AM-AFM, as demonstrated in the seminal paper on FM-AFM by Albrecht *et al* [24].

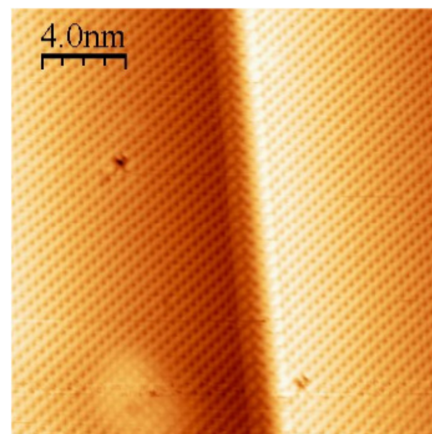

Figure 3. Atomically resolved NC-AFM image of KBr(001) surfaces showing a monoatomic step and atomic defects.

True atomic resolution was first obtained in NC-AFM by Giessibl [25] and Kitamura and Iwatsuki [26] in 1995. It has now been achieved on a wide variety of surfaces (metals, covalent or ionic semiconductors, covalent or ionic insulators) and the technique, after being used in UHV for a long time, is now adapted to ambient conditions and to liquids, especially for applications in biology [27]. Referring to table 1, true atomic resolution has been obtained on KBr(001) (figure 3) [28] and many other alkali halides [29], MgO(001) [30], $Al_2O_3(0001)$ [31], $CaF_2(111)$ [32] but not yet on SiC, GaN and AlN.

Even less is reported on the imaging of molecules on the surface of the materials of table 1 by NC-AFM. Most of the reported work was performed on alkali halide surfaces, such as KBr(001), and at room temperature [33]. In these conditions, for low coverage, most molecules diffuse, due to their weak interaction with these surfaces, making the observation of single isolated molecules impossible, except when adsorbed on a defect, for instance a step edge. Using structured surfaces [34] allows a more efficient trapping of the molecules [35]. For higher coverage, monolayer islands followed by multilayer 3D crystallites are often observed (PTCDA on NaCl(001) [36] and on KCl(001) [37]). Molecular lines are also formed in certain cases (DiMe-PTCDI/KBr(001) [38]).

It is clear that NC-AFM will boost this rapidly developing new domain of surface science. With the advent of low temperature NC-AFM heads, these problems of mobility of molecules on insulating surfaces will become less limiting. Nevertheless, a large effort is needed to synthesize molecules adapted to room temperature experiments in the longer-term vision of devices that should ideally work at this temperature.

3.1.3. Atomic scale surface interconnection circuit. The next step in the interconnection strategy presented in figure 2(b)

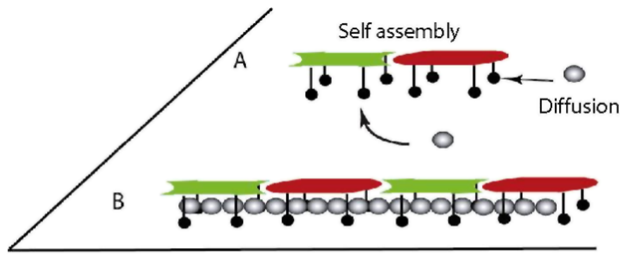

Figure 4. The 2 step self-assembly process for the fabrication of a long metallo-organic molecular wire stabilizing metal atomic wires at the surface of an insulator. (A) 2 types (gray and black) of Lander molecule self-assembled at the surface of the insulator in a very long molecular chain. (B) The metallo-organic molecular wire is assembled by surface diffusion during (or after) the molecule Lander building block sublimation (adapted from The Pico-Inside European project final report. www.phantom.com/pico-inside).

is to build conductive atomic wires on the surface of the wide gap material to connect the atomic scale circuit to the metallic nanopads, as presented in figure 2(b). Therefore, it is not enough to use, for example, surface step edges to self-stabilize metal atomic wires following a peculiar surface crystalline direction. These atomic wires have to converge toward a specific surface location whose lateral dimension will be around 10 nm and this is generally not compatible with surface crystallographic directions. Two strategies have been envisioned to construct these atomic wires: single atomic manipulation or a self-assembly process via molecular molding.

Theoretical works suggest that it should be possible to manipulate single atoms [39, 40] and molecules [41] on insulating surfaces. The simulated manipulation process generally requires a very precise positioning of the tip that is becoming achievable, at least with the recent low temperature NC-AFM. The first well-controlled atom manipulation experiments using NC-AFM were reported very recently on semiconducting surfaces in the vertical [42] and in the lateral mode [43]. Poorly controlled manipulation of an unknown species was also reported on $CaF_2(111)$ [44]. It is thus likely that controlled manipulations of single metal atoms and molecules on the surface of an insulating material will become possible in the near future. Notice that it is not sufficient to build a conductive line. It must be stable as such. It turns out that metallic cohesion does not help much in this regard since there is generally a mismatch between the inter-atomic distance that 2 metallic atoms must adopt on an insulating surface for the complete atomic wire to be conductive and the distance for 2 metallic atoms to remain stable at their adsorption site selected by atom manipulation. On NaCl(001), the distance between two gold atoms in a chain should not be less than 0.7 nm for the chain to maintain its stability [40]. Such a distance is too large for the conductance of this atomic wire to reach at least one quantum of conductance [45].

To circumvent this problem, one solution is to create atomic scale defects at the surface of the wide gap material by atom extraction. This is a not so well explored area and only e-beam destructive pits on alkali halides have been made to test how metal atoms can be successfully stabilized at the edge of those pits [46]. The other solution is to play with the recently discovered ability of certain well designed organic molecules to mold metallic atoms [47] and even to surface extrude a single well shaped atomic wire from a step edge [48]. This molecular property was discovered on plain metal surfaces using LT-UHV-STM single molecule manipulation. It is now explored in a more systematic way by designing Lander molecules that can self-assemble in long molecular chains, first on a metal surface [49], and then on an insulating surface [50]. It is expected that the co-evaporation of metal atoms with these Lander molecules on an insulating surface self-assemble into long metallo-organic molecular wires with a good conductance (figure 4). After such a self-assembly, it remains to manipulate these molecular wires one at a time to position them with respect to the interconnection architecture. It may also turn out that surface chemistry, where monomers of low gap molecular wires are sublimated on a surface, can help in a surface reaction, where under an increase of the surface temperature, a fully covalently bonded molecular wire is synthesized at the surface of an insulator, ready to be AFM manipulated in the suitable surface interconnection configuration [44]. These surface chemistry processes have been already experimented with on metal surfaces [51] under the STM and are ready to be transferred under a NC-AFM for wide gap surfaces. In this case, the dynamic nanostencil technique (see section 3.3) will help in delimiting the part of the surface on which the chemical reaction will occur.

3.2. Metallic nanopad fabrication and re-configuration (level B)

The metallic nanopads (B) of the figure 2(b) interconnects have 2 functions: first, they serve to bridge the atomic scale circuit (A) to the next mesoscopic level of interconnection (C). Second, they provide the metallic density of states necessary in a decoherence like process to superpose the billions of through bond electron transfers per second that are occurring between a couple of voltage bias nanopads (B) in the atomic scale circuit (A). This superposition results in the tunneling current intensity which can be measured with a standard ammeter [52]. The pad lateral dimension must be compatible with the actual precision of the dynamic nanostencil technique (described in section 3.3), which is of the order of a few tens of nanometers. These nanopads should also be not too high for the AFM tip to be able to image the surface where the central atomic scale circuit is located and should be crystalline to present well-defined facets without which imaging a molecule becomes very difficult.

The first classification of growth modes of a deposit on a surface was proposed by Bauer [53], who distinguished 3 basic modes: (i) the Frank–van der Merwe two-dimensional growth, where atomic layers are formed one after each other, (ii) the island Volmer–Weber growth, where three-dimensional clusters are formed and (iii) the Stranski–Krastanov mode, where two-dimensional growth is followed by cluster formation. A fourth mode was introduced later: the reactive mode, where an interphase is formed between

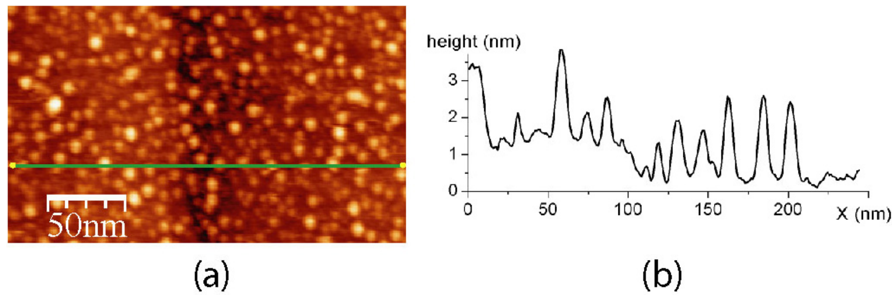

Figure 5. (a) AFM image of an alumina surface where 4 ML of copper have been deposited at room temperature. (b) Profile corresponding to the line plotted on the image.

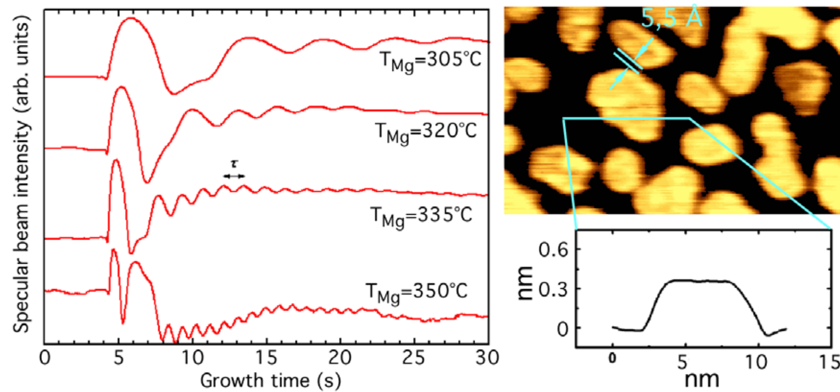

Figure 6. Mg metallic nano-island growth on the GaN(0001) surface. Left: the RHEED oscillations at different substrate temperatures during the growth. Right: UHV-STM image of a 0.6 ML deposit showing Mg monolayer islands with very small inter-island distances. Adapted from [55].

the substrate and the deposit as a consequence of a chemical reaction or inter-diffusion at the interface.

It turns out that, in most cases, metals grow on the materials listed in table 1 in the Volmer–Weber mode, that is in the form of low aspect ratio clusters. This is particularly the case for alkali halides and most oxide surfaces, while much less is known on the other materials. An example is shown in figure 5, where 4 monolayers (ML) of copper were deposited at room temperature on a Al_2O_3(0001) surface and imaged with AFM: compact islands with sizes ranging from 2 to 6 nm are observed. This general behavior can be traced back to the fact that the surface free energy of insulating materials is quite generally much lower than that of metals. Of course, many other parameters influence the growth mode, such as the lattice mismatch between the two materials or the nature of the interface (reactive or not) as well as the experimental conditions during the growth, which can drive the system far from thermodynamic equilibrium. We refer for a detailed description to the book of Noguera [54].

From a practical point of view, this behavior constitutes a serious problem to make suitable nanopads. Fortunately, it was recently demonstrated that Mg grows on the N-rich face of GaN(0001) in the layer-by-layer mode [55], making this system promising for our purpose. Figure 6 shows the RHEED oscillations during the growth at different temperatures and a STM picture showing monolayer (height $\sim$0.3 nm) epitaxial islands. This behavior is favored by the small lattice parameter mismatch of 0.3% between the substrate and the deposit. Note that STM imaging can be practiced on GaN, due to its relatively small band gap (table 1). In contrast, studies to find a metal that would grow in the layer-by-layer mode on AlN, which has a larger gap (table 1), require the use of NC-AFM.

Aside from continuing the exploration of the growth conditions of metal nano-islands on large gap semiconducting and insulating surfaces, for example by playing with kinetic effects to better adapt the metal nano-island shape, it is also important to consider how to arrange them on the surface. In figures 5 and 6, they are randomly distributed over the surface, which may be very good to find 2 nanopad contacts as indicated in figure 6 with sometimes very small inter-nanopad distances below 1 nm. Such small gaps are impossible to fabricate with conventional e-beam nanolithography techniques. For a larger number N of interconnects, the nanopads will have to be arranged in a specific order and orientation on the insulating surface. At present, the only way to construct such an interconnection structures, with for example N nanopads converging in a circle toward the same surface spot, is to manipulate them one-by-one using the tip of a NC-AFM. This puts forward the need to study manipulation by NC-AFM, not only of single atoms or molecules, but also of larger nano-objects made of millions of identical atoms. This had already been demonstrated on a small gap semiconductor surface with

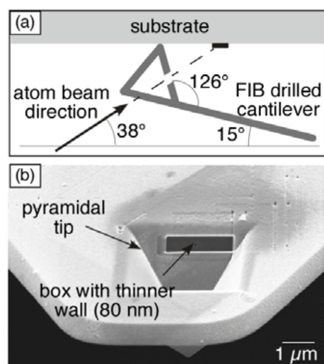

Figure 7. (a) Schematic view of the geometrical configuration for the Toulouse AFM nanostencil machine. (b) Scanning electron microscopy (SEM) image showing a recessed box in the rear face of an AFM tip, which was first thinned down to 80 nm by FIB. Adapted from [59].

STM (see section 4) and is now required for larger electronic gap surfaces.

3.3. The interconnections from the nano- to macroworld (levels C2, D and E).

According to the interconnection scheme illustrated in figure 2(b), and after having fabricated well faceted metallic nano-islands (nanopads), the next steps are the realization of the three interconnection levels C2, D and E with increasing width from the nanometer to the macroscopic scale. To realize these electrodes on the surface, it is not possible to use either a resist based nanolithography technique or a stamping technique because the atomic cleanness of the working area where the atomic scale circuitry A and the nanopads B should be built should be preserved. The only remaining possibility is to use different stencil techniques under UHV to grow the nanoscale wires (C2) and the microelectrodes (D), and then to use metallic microcantilevers (E) to contact the microelectrodes. The order in which these different operations have to be performed does not follow the order in which they were presented in section 2, but depends on technical constraints related to the necessity of successive alignments of the different structures. The operations performed to realize the interconnection levels C2, D and E, described in this section are combined with levels A and B described in sections 3.1 and 3.2 according to the following sequence:

(1) Surface preparation, for instance growth of AlN.
(2) Growth and possibly manipulation of the metallic nanopads (level B).
(3) Growth of the microelectrodes by static stenciling (level D).
(4) Nanostencil deposition of the nanowires between the metallic nanopads and the end of the microelectrodes (level C2).
(5) Building of the atomic scale circuitry by NC-AFM (level A).
(6) Electrical measurement of the molecule properties with the help of metallic microcantilevers (level E).

3.3.1. The stencil techniques. Two main stencil techniques exist: the static technique, in which the mask is placed in contact with the substrate and the pattern is directly evaporated on its surface, and the dynamic technique [56–60], in which the pattern is drawn on the substrate by moving the mask. This last mode is generally implemented on an AFM microscope. Indeed an AFM cantilever can be patterned using the focused ion beam (FIB) technique and used as the shadow mask. The principle of the nanostencil technique based on an AFM cantilever is presented in figure 7.

Figure 7(a) shows the geometrical configuration of the dynamic stencil on the Toulouse machine. Si_3N_4 cantilevers, with hollow tips, are used. The stencil pattern is made in the rear side of the tip, using a focused gallium beam. It should be positioned as close as possible to the substrate in order to minimize the geometrical enlargement of the deposited pattern, which varies as the ratio between the pattern–surface distance and the evaporation source–surface distance. To reach small mask pattern sizes, it is also necessary to thin down an area of the tip side from about 800 to 80 nm (the box displayed in figure 7(b)) before drilling the patterns in this membrane.

The high positioning precision of the AFM combined to the nanometric size of the apertures made in the AFM cantilever allows one to obtain nanowires. The dynamic nanostencil is a UHV *in situ* technique with the additional advantage of allowing the imaging of the surface at the different stages of the fabrication process and therefore directly aligning the mask relative to the nanopads.

As demonstrated in different works, one of the difficulties of the stencil techniques is that the apertures tend to clog rapidly [60–62]. This well-known phenomenon is the main disadvantage of the nanostencil process. One solution is to use self-assembled monolayers (SAM) to passivate the surface of the cantilever. It has been demonstrated that alkyl or perfluoroalkyl terminated SAMs delay the clogging of the stencil by reducing the adhesion of the deposited metal inside the nanostencil apertures [61, 63]. The use of wet etching to eliminate the clogging of stencils after gold or aluminum evaporation has been reported as well [64, 65].

3.3.2. Growth of the microelectrodes by the static stencil technique. The microelectrodes are deposited in UHV by the static stencil technique. Specific microelectrodes were designed in such a way that they are protected by the shadow of the AFM cantilever used during the next steps to grow the nanowires.

Figure 8(a) presents the microelectrodes stencil mask, observed by optical microscopy. One microelectrodes device constitutes the bridge between level C2 (1 μm) and E (10 μm): the pads used for the connection with the metallic microcantilevers are 6 μm in width separated by 6 μm. So the total device is 62 μm $\times$ 20 μm. It is easily seen with an optical microscope, but also with the wide scan range AFM available with the Microclean Room developed in Toulouse, described in section 3.3.5. A 75 μm $\times$ 75 μm NC-AFM image of one device, made by depositing copper on SiO_2 [60] is displayed in figure 8(b).

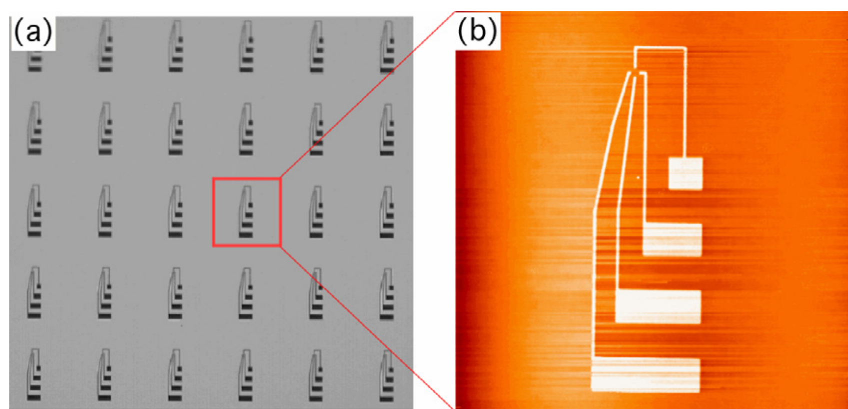

Figure 8. (a) Optical microscope image of the microelectrodes aperture made in a static stencil membrane (b) 75 μm × 75 μm AFM image in the non-contact mode showing one device [60].

3.3.3. Growth of the nanoelectrodes by the dynamic nanostencil technique. The nanopatterning of the inter-microelectrodes area by the nanostencil technique, described previously, relies on the precise determination of the actual location of the deposited nanopattern with respect to the nanostencil AFM tip. Consequently, a preliminary calibration step is needed for each new nanostencil AFM cantilever. In a typical calibration experiment, the cantilever is approached to a bare substrate in either non-contact or contact AFM mode. A deposit is then made using the dedicated effusion cell. Large scale AFM images are then obtained by scanning the X–Y table and the relative position of the deposited pattern and the AFM tip can be precisely measured. Subsequently, the bare substrate is exchanged with the substrate with the deposited microelectrodes. Hence, knowing the location of one set of microelectrodes and the relative position of the deposit with respect to the AFM tip apex, the nanopositioning table is moved so as to deposit the nanopatterns precisely between the microelectrodes. Figure 9 shows an NC-AFM image of 5 nm thick copper nanoelectrodes deposited between the 4 microelectrodes.

This example shows the difficulties met for precise alignment: the nanoelectrodes pattern is correctly aligned in the y direction but has a misaligning of around 100 nm in x direction and a defect angle of 10°. The error in the x and y direction is related to the mechanical drift of the piezoelectric tube during the experiment. The angle error comes from addition of error angles during the FIB drilling and the gluing of the cantilever on its holder. We are confident that these errors can be minimized and plan to improve the overall accuracy to 20 nm, which is the limit imposed by our wide range (XY) table (see section 3.3.5).

3.3.4. Electric measurements with the microcantilevers. The micropads at the end of the microelectrodes (figure 8) should be connected to the macroscopic world. Metallic microcantilevers mounted on a specific UHV compatible printed circuit board (PCB) connected to the outside of the UHV chamber are used for that purpose. They should have good mechanical and electrical properties in order to establish low resistance electrical contacts with the micropads. The

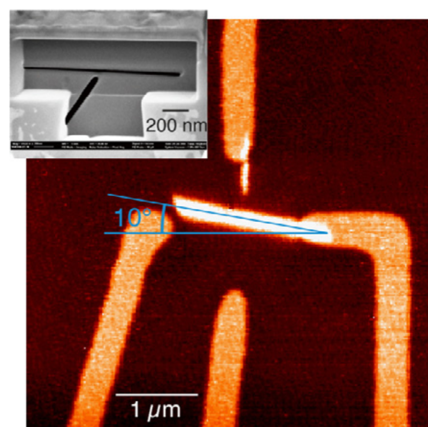

Figure 9. Non-contact AFM image (4 μm × 4 μm) of Cu nanoelectrodes deposited between the Pd microelectrodes made by a static stencil on a Si substrate; (inset) SEM image of the FIB drilled pattern distorted to correct the geometrical distortions due to the evaporation geometry. Adapted from [59].

first models of these metallic microcantilevers used in air were made entirely with gold and have shown bad mechanical properties: they are easily plastically deformed. In more recent designs, 1 μm thick SiC layers were used to support metallic wires. To avoid contact problems, it was also necessary to induce a curvature of several μm of the SiC cantilevers [66]. Furthermore, the size should be correctly chosen for the microcantilevers to be easily seen with the optical microscope. In the particular case of the Microclean Room, the size of the microcombs is 6 μm in width for SiC, 4 μm in width for each metallic wire, 100 μm in length and 24 μm in periodicity. Figure 10 shows a microcomb mounted on its dedicated PCB.

3.3.5. The Toulouse setup. To realize under UHV the 5 levels of interconnect described in figure 2(b), the deposition of molecules, their observation by NC-AFM and the measurement of their electrical properties, the GNS group has designed and realized a dedicated UHV equipment called DUF (DiNaMo UHV Factory). This equipment allows the transfer of samples under UHV between five complementary UHV chambers:

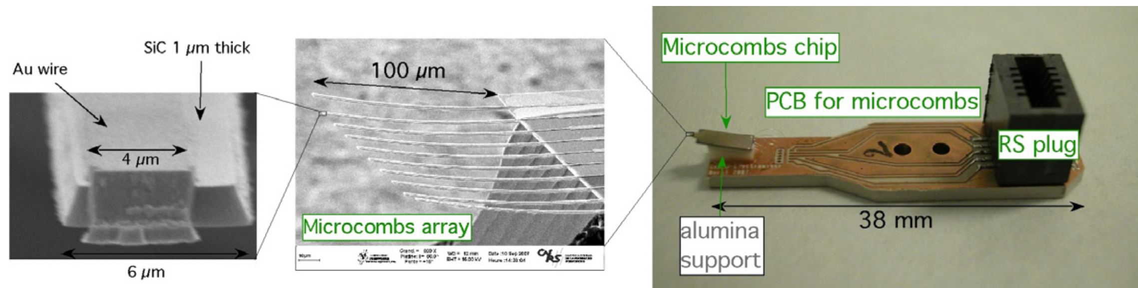

Figure 10. (left) SEM image of the end of a SiC based cantilever with the Au wire; (middle) SEM image of the microcombs made of a 10 SiC based cantilever; (right) microcombs chip mounted on its specific PCB. The SiC based microcombs were made by the LPN (CNRS UPR20) at Marcoussis during the DiNaMo project (French ANR founding No ANR-05-NANO-014).

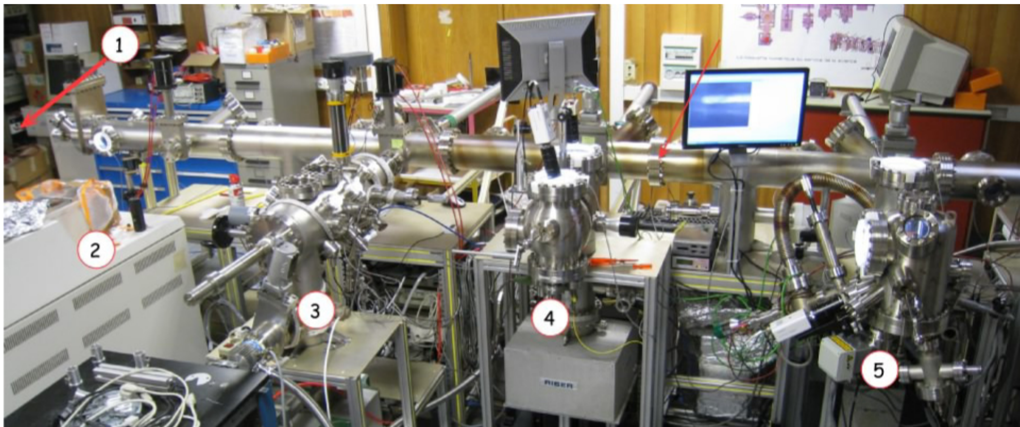

Figure 11. The DUF (DiNaMo UHV Factory) equipment allows the transfer of samples between 5 complementary UHV chambers in order to realize the 5 levels of interconnect on wide band gap semiconductors (GaN, AlN). The different chambers are described in the text.

(1) MBE growth dedicated to nitride semiconductor growth, metallic nanopad growth and stencil evaporation for microelectrodes.
(2) Mass spectrometer transformed in a molecular ion source.
(3) Preparation chamber for clean substrates, STM tips and AFM cantilevers.
(4) Room temperature AFM/STM for surface characterization by STM and NC-AFM.
(5) The microclean room: AFM/STM modified for nanostenciling experiments and electrical measurements.

Figure 11 shows this equipment in its actual state.

To realize the steps 4 and 6 described in the previous section, a UHV Omicron Nanotechnology VT STM/AFM head has been modified to accommodate different tools, namely [60]:

(1) A flexural-hinge-guided (XY) piezoceramic driven nanopositioner stage (100 μm $\times$ 100 μm, repeatability 5 nm) with a closed loop control based on capacitive sensors,
(2) An evaporation system highly collimated on the cantilever to perform nanostencil deposition,
(3) A (XYZ) piezo-table for positioning the metallic microcombs,
(4) An optical microscope to control the positioning of the microcombs.

These modifications were designed by the mechanical department of the laboratory. Figure 12 shows a scheme (a) and a picture (b) of the modified AFM.

The main advantage of using a commercial UHV AFM/STM is to benefit from its good characteristics for SPM imaging. But the piezoelectric tube used to scan has a range of a few μm only. The addition of an XY table to move the sample offers the possibility to perform wide range scanning, up to 80 μm SPM images, while keeping the possibility to realize atomic scale imaging with the piezoelectric tube.

One of the disadvantages is the small accessible space around the SPM head. Indeed, it is not possible to place an optical microscope with normal incidence with respect to the substrate, and an atomic source for the nanostencil experiments with normal incidence with respect to the AFM cantilever. In our case, the image obtained by the optical microscope is reflected by a mirror that makes an angle of 30° with the substrate plane. This gives distorted images, with a loss of resolution: only 3 μm instead of 1 μm in normal incidence. The effusion cell is fixed on a port of the UHV chamber at an angle of 33° with the horizontal plane, and another at an angle of 28° between the two vertical planes passing through the evaporation beam and the central axis of the cantilever (figure 7(a)). This orientation of the atom beam induces distortion, which should be taken into account in the design

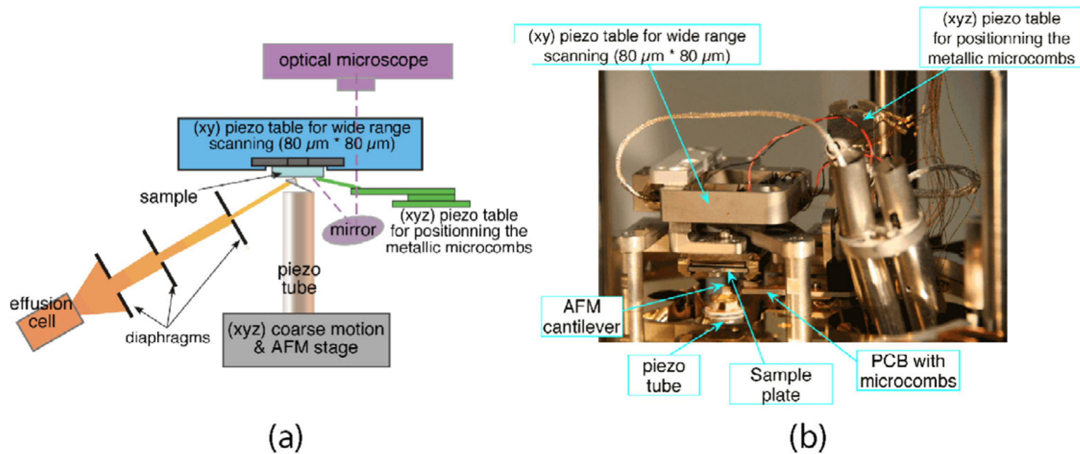

Figure 12. (a) Schematic view of the functionalities implemented inside the microclean room and (b) the modified AFM/STM head.

of the nanopattern to be drilled into the pyramidal tip of the cantilever (figure 9) [60].

4. Small VB–CB electronic gap surfaces

As presented in figure 2(c), a small electronic gap (below a few eV) of the surface material supporting the interconnection structure leads to only 3 levels of interconnects. As in section 3, levels (A) and (B) depend on the mastering of atomic scale surface science phenomena while level (C1) relies on the ability to fabricate multiple ultra-sharp metallic tips to contact each metallic nano-island of level (B). The constraint with a multi-access interconnection technology on a small electronic gap surface material is to avoid surface leakage currents between the electrodes contacting the surface metallic nano-islands. Therefore, it is compulsory to contact these nano-islands from the top. This constraint has a lot of consequences for the structure of the interconnection machine depicted in figure 2(c). In particular, a scanning electron microscope is required instead of the figure 2(b) optical microscope because the lateral size of the nano-islands is necessarily very small to avoid inter-nano-island leakage currents. In this section, progress and problems that remain to be solved for these 3 levels of interconnections are presented up to the description of the interconnection machine in construction at IMRE in Singapore, which is devoted to these small gap supporting materials.

4.1. Semiconductor surface preparation

The preparation of a semiconductor surface usually begins by degassing and destroying the oxide layer. The surface is then annealed by passing through the sample a current whose intensity depends on the doping level of the bulk material [68]. These preparation conditions have to be carefully optimized to get the necessary large atomically flat terraces, in the 50 nm width range and with a homogeneous reconstruction all along a terrace. A problem is that such surfaces are usually very reactive, due to the presence of dangling bonds. Even under very strict UHV conditions, they get contaminated on the timescale needed to build the atomic scale circuitry and its connections, which is at least of the order of a few hours. Saturating these surfaces by adsorbing hydrogen, chlorine, sulfur or small molecules is an efficient solution to preserve their integrity on this timescale [69]. In many cases, this modification has the additional benefit of increasing the electronic surface band gap. For example the native Si(100) surface gap of 1.2 eV increases to 2.1 eV with an hydrogen saturation in its 2×1 reconstruction phase [67]. It was demonstrated recently [75] that this saturation layer can also decouple electronically a conjugated molecule from the Si(100) surface similarly to what was observed for an ultra-thin ionic insulator on a metal surface [76]. This electronic decoupling is very important because, on such a surface, the only way to interconnect a molecule with an atomic precision is to fabricate surface atomic wires (see section 4.2 hereafter) and to STM manipulate the molecule between them, restoring the coupling of the molecule to both ends of these wires as proposed in figure 2 for the atomic circuit A. A limitation of this approach for the next processing steps is that these saturation layers have a limited thermal stability (for instance 300–400 °C for Si(100) 2×1-H [70]).

There are a few semiconductor surfaces where this saturation can be considered as part of the material structure. This is the case of lamellar semiconductors like MoS_2. In this case, the sulfur overlayer is hardly bonded to the Mo atoms underneath. The $MoS_2(0001)$ surface is rather easy to prepare by a fast UHV cleaning followed by a standard surface preparation temperature in the 300 °C range [71]. The extension of the atomically flat surface of lamellar compounds is usually rather large, up to a few microns in lateral extension in some cases. MoS_2 is one of the most interesting materials of the lamellar compound series with a bulk gap around 1.3 eV and a surface gap in the 1.0 eV range [72]. The MoS_2 surface remains atomically perfect and flat up to 1100 K. Above 1200 K, a reconstruction of the top layers of MoS_2 to Mo_2S_3 is observed, leading to one-dimensional atomic double rows on the reconstructed surface [73]. Such temperature stability is very important for the fabrication of surface atomic wires by STM extracting rows of sulfur atoms. The drawback is that it is

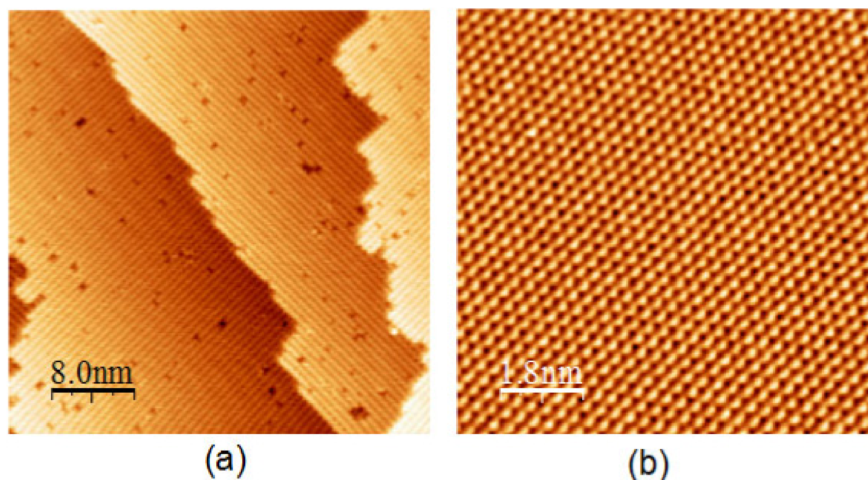

Figure 13. STM images of a Si(100) 2 × 1 and a MoS_2(0001) surface showing atomic resolution before the start of any construction or fabrication steps. As described in this section (and in section 3 for large gap surface materials), these construction and fabrication procedures must be carefully tested in such a way that atomic resolution is kept up to the multi-probe I–V measurements step. (a) The Si(100) surface was prepared with the objective of increasing the terrace size before the hydrogenation step. (b) The MoS_2 surface was prepared to determine the experimental conditions to extract the sulfur surface atoms one-by-one.

extremely difficult to extract these surface atoms as compared to the surface atoms of the Si(100) 2 × 1-H surface [74]. There is a crucial need for a material stable enough in temperature and whose surface atom chemical stability is between Si(100)-H and MoS_2.

STM images of the 2 principal surfaces used at IMRE in Singapore to explore atomic scale interconnection are presented in figure 13, each showing a clear atomic resolution. One imaging problem comes from the softness of lamellar semiconductor materials in the direction perpendicular to the surface. The sample is then easily deformed by the force that the tip exerts on the surface during imaging. In this situation, adsorbates or metallic nano-islands can be easily brushed away by the tip because the tip apex to surface distance can be very small during STM imaging [71].

4.2. Atomic scale surface interconnection circuit

At the passivated surface of a semiconductor, the STM fabrication of atomic wires is facilitated because the created or the native dangling bond atom saturation can be manipulated atom by atom to create a line of surface dangling bonds [14]. It was theoretically predicted that a perfect row of surface dangling bonds introduces at least one conduction band in the electronic surface gap induced by the passivation layer [77]. The effective conductance of this dangling bonds electronic path will certainly depend on the doping of the substrate and around the surface Fermi level, its dispersion is generally much less that 1 eV, making the corresponding carrier effective mass quite large. The detailed molecular orbital composition of such dangling bonds lines is generally complex because it involves the liberated atomic orbital per surface atom plus the contribution of the nearby atoms whose orbital hybridization may have been changed too [72]. Even with a conduction band width smaller than 1 eV, a ballistic channel of conduction requires the fabrication of a long line of dangling bonds. If the line is too short between the molecule to be contacted and the metallic pad, it remains a quantum box with its characteristic discrete electronic resonances, on average one or two per extracted atom [72, 77]. Mastering the fabrication of long lines of dangling bonds is also very important for the inter-metallic nanopad (B) distances to be large enough to minimize the surface tunneling leakage current intensity between them.

Surface atoms saturating the dangling bonds of a semiconductor surface have a bonding energy around a few eV [14]. Therefore, a voltage pulse of a few volts applied between the tip and the surface is able to destabilize a given surface atom [14, 74]. This is a vertical manipulation process since, in many cases, the extracted surface atom is desorbed from the surface and reaches the apex and, eventually, by subsequent tip surface diffusion, the body of the tip. It depends on the surface material but also whether or not an electronic resonant state of the surface is accessible for the selected tip–surface bias voltage. In many cases, the main desorption process requires the resonant excitation of the anti-bonding state of the surface atom [14]. Another mechanism, active for large tunneling currents, involves the vibrational excitation of the atom surface bond by inelastic tunneling.

Using this vertical manipulation technique, writing lines of surface dangling bonds at the atomic scale has been practiced by a few groups up to the point where atomic scale circuits could be constructed atom-by-atom [14]. The first single atom desorption experiments were reported on a non-saturated Si(111) surface [78], then on a hydrogen passivated Si(100) surface [79] and then on a MoS_2 surface [74]. What is not yet known is the number of atoms the same tip apex can extract before being chemically transformed and becoming inactive for the vertical manipulation process. The drawback of this vertical manipulation technique is that some extracted atoms already adsorbed on the tip apex can be transferred again and re-saturate some dangling bonds of the already fabricated line. Here, there is a clear need for a better understanding

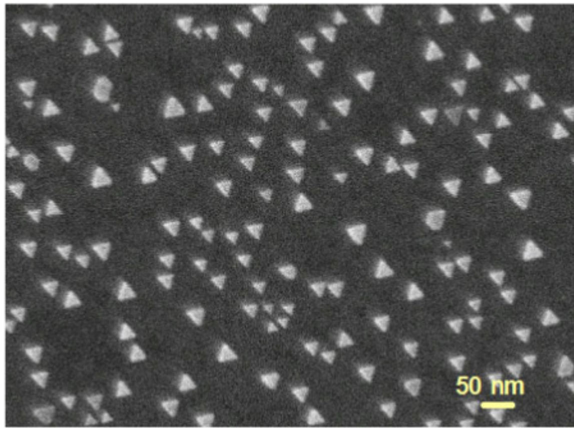

Figure 14. SEM image of the distribution of Au nano-islands on $MoS_2(0001)$ after the fabrication process detailed in section 4.3. Many islands are 30 nm in lateral size. Notice also the very sharp summits of these triangles.

of these extraction and re-saturation processes together with a good understanding of the lateral surface diffusion processes occurring on the surface while a newly created dangling bond is re-saturated by a nearby saturating atom jumping over.

4.3. Metallic nanopads fabrication and re-configuration

The metallic nanopads (B) in figure 2(c) are necessary to pass from the surface atomic wires made of dangling bond lines to the metallic tip apex (C1). This very local metallization must be practiced directly on the passivated semiconductor surface. It turns out that there are not a lot of passivated surfaces whose passivation overlayer can sustain the temperature required for metallization [80]. These temperatures, which are usually higher that a few hundred degrees, locally destroy the passivation layer. One solution to this problem is to start with a robust semiconductor surface like MoS_2 and then to transfer the metallic nano-islands onto another surface by contact printing in UHV [81].

On the $MoS_2(0001)$ surface, gold atoms form triangular nano-islands whose lateral dimension can go down to 5 nm for a thickness of a few nm [71]. An optimum of 30 nm lateral and 10 nm in height can be easily obtained by tuning the surface temperature during the metal evaporation [71]. In a standard preparation, MoS_2 wafers are fabricated from bulk molybdenite stones directly mined in Australia. The slides are cut into 10×10 mm^2 pieces. The top surface of a MoS_2 slide is cleaved and immediately loaded into a thermal evaporator. After the sample is outgassed at 400 °C for 3 h, Au is thermally evaporated onto the MoS_2 surface at 400 °C with a deposition rate of 0.02 nm s^{-1}. The total thickness of evaporated Au, monitored by a quartz microbalance, can be kept as low as 1 nm. After Au deposition, the sample is maintained at 400 °C for another 1 h to facilitate the formation of the nano-islands. During this process, the pressure in the chamber must be below 2×10^{-5} Pa. The nano-island growth conditions can be optimized to achieve a majority of nano-islands being of equilateral triangular shape with a 20–30 nm lateral size (see figure 14).

Such a fabrication and self-assembly process usually leads to a rather homogeneous distribution of Au islands. In some cases, the apices of 2 islands can be face-to-face at distances as low as a few nanometers, constituting an ultra-clean and atomically well-ordered nano-junction to interconnect a single molecule since the background surface has generally kept its atomic scale corrugation. Unfortunately, the $MoS_2(001)$ electronic surface band gap is too small for the 'island-surface-island' conductance to be much smaller than the one of a conjugated molecule to be interconnected. Therefore, instead of searching on the surface for a multi-pad configuration adapted to such conductance measurements with the good inter-pad distance, we have learnt the conditions to manipulate these nano-islands one-by-one on the MoS_2 surface [71]. There are 2 modes of manipulation. In the soft one, the tip apex does not mechanically touch the nano-island but is charging it. A large number of scans is necessary to charge a nano-island enough for the electrostatic force between the STM tip apex and the nano-island to be large enough for the nano-island to move away, but with a precision better than 0.1 nm [71]. In the mechanical mode, the tip apex is simply pushing on a facet of the nano-island. This mode of manipulation is less precise (1 nm or more) but very fast [71]. Figure 15 presents a few examples of Au nanopad nanostructures constructed by manipulating the nano-islands one after the other.

Starting from a flat MoS_2 surface, these nanostructures cannot be transferred as such by a direct contact printing between this surface and a larger gap semiconductor surface. Firstly, the construction will be deformed during the printing. Secondly, for interconnecting a surface dangling bond interconnecting circuit, it is better to manipulate the nano-islands after the fabrication of the surface atomic wires. In this way, a given metallic nano-island can be manipulated step-by-step over the corresponding atomic wire up to the point where the conductance is larger than the surface leakage conductance. We have recently demonstrated that Au nano-islands can be transferred to an Si(100)-H surface after a specific MoS_2 surface microscale structuration [81]. The MoS_2 surface must be structured in micronscale pillars creating a matrix of stamps. We have shown that Au nano-islands can be fabricated on the surface of each pillar after changing the characteristic fabrication temperature. A 10% overall transfer rate to Si(100)-H was obtained for 10–20 μm lateral size pillars. The experimental conditions to manipulate these nano-islands on the Si(100) 2×1-H surface, as it was done on the MoS_2 surface, remain to be determined. Notice also that the hydrostatic pressure during transfer printing must be optimized to preserve the hydrogen passivation layer under the nano-islands.

4.4. Tip apex fabrication

Fabrication of atomically clean nano-probes in a highly controlled manner with diameters in the range of 2–5 nm is crucial for contacting metallic nano-islands positioned in close proximity on the surface of a semiconductor, as presented in figure 15. Furthermore, these ultra-small tips must have a very high aspect ratio to be able to increase the number of tips

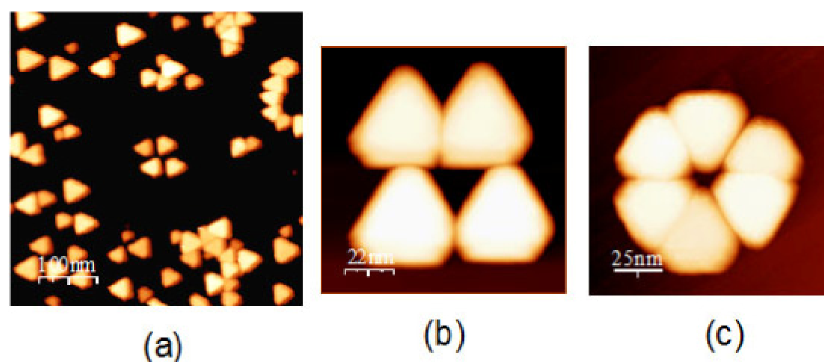

Figure 15. Example of contacting nanostructures constructed by manipulating the nano-islands one after the other in a lateral STM manipulation mode on the $MoS_2(0001)$ surface. (a) More than 50 nano-islands have been manipulated around to assemble the central 4 contacting nanostructure. (b) Zoom on a construction of 4 nano-islands manipulated in a square. (c) Zoom on a construction of a 6 nano-islands interconnection structure converging toward a 12 nm central active area where the atomic circuit is supposed to have been atomically fabricated before this construction. (a)–(c) are UHV-STM images with $V = 0.2$ V and $I = 10$ pA.

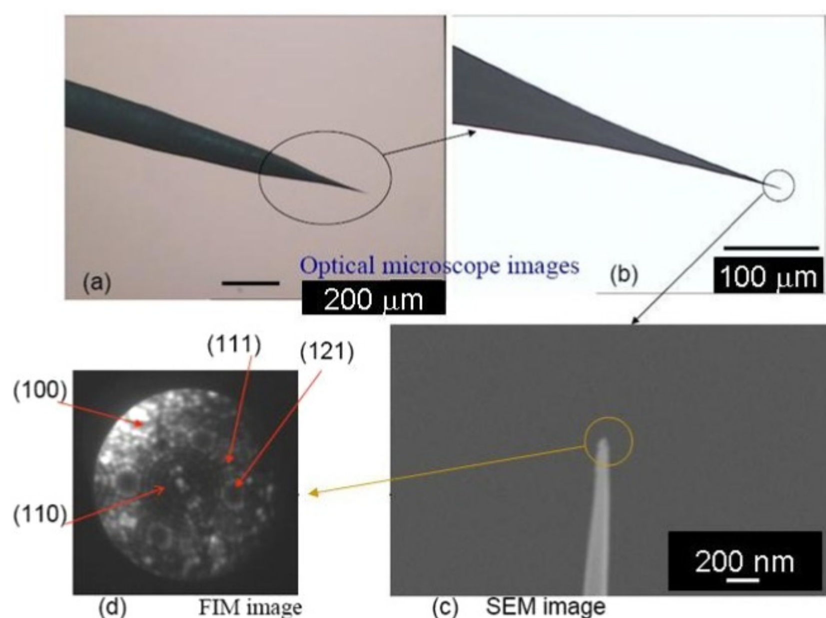

Figure 16. Two optical microscope images with different magnifications (a) and (b) and a SM image (c) of a very sharp tungsten tip electrochemically prepared before being FIM imaged. The presented FIM image (d) shows circular arrangements of W atoms corresponding to specific crystallographic orientations at the end of the tip apex.

that should converge towards the same nanoscale area of the surface, as for example the 6 nanopads configuration presented in figure 15. To ensure a rigorous cleanliness of these tips and to precisely determine the tip size and shape, a field ion microscope (FIM) is used to shape atom-by-atom the tip apex using the spatially controlled electric field assisted technique and at the same time to be able to image with an atomic scale precision the fabricated tip apex.

Invented by Muller in 1956 [82], the FIM is based on placing, in a UHV chamber, a sharp tip (generally in tungsten), with a typical radius of curvature of 100 nm, in front of a phosphor screen. Such 100 nm tip apices are usually prepared by AC electrochemical etching as illustrated in figure 16. When a high voltage, in the range of 5–20 kV is applied, a high electric field in the order of 5 V $Å^{-1}$ is generated at the tip apex. This field is adequate to ionize an inert atom gas (for instance He) introduced in the FIM chamber. Once a He atom is ionized at the tip apex, it is expelled towards the screen where it is detected as a bright spot. As these events take place all over the tip apex surface, a stereographic projection of the tip surface atomic structure appears on the screen. The optimum image contrast is attained when the tip is cooled to liquid nitrogen temperature, since the ionization probability and atom surface atom stability are improved, as presented in figure 16(d).

The tip radius of a standard clean tip is calculated by identifying two atomic poles and counting the number of atomic rings between the centers of consecutive planes. For the tungsten tip of figure 16, this gives a 12.8 nm tip radius of curvature.

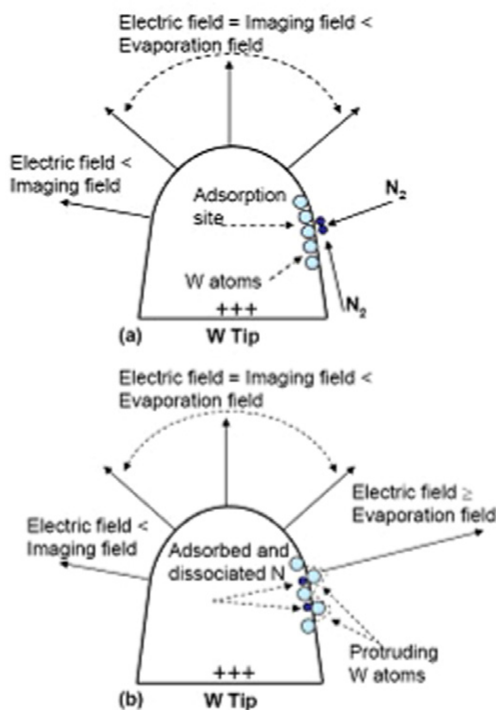

Figure 17. Schematic illustration of the electric field assisted technique where N_2 is adsorbed on the tip body, decomposed, and during the decomposition expels metal atoms from the tip apex [85].

To contact a 30 nm nanopad (figure 15), the tip apex radius needs to be reduced below 5 nm. Under an SEM microscope, this will ease the alignment of each tip apex with a given nano-island before contacting it. Such a reduction of the tip radius of curvature can be achieved by using the surface electric field assisted technique [84]. This technique depends on the introduction of a small amount of N_2 gas into the FIM chamber just after the preparation of an atomically clean broad tip as presented in figure 16. Notice that nitrogen has a smaller ionization barrier (14.5 eV) than helium (24.5 eV). Therefore, nitrogen atoms cannot reach the apex where the electric field is maintained at the best imaging conditions for ionizing He because they will be ionized before that. In these conditions, N_2 prefers to settle down on the shank where the field is much lower. On a W surface, it is well known that N_2 dissociates and subsequently diffuses into the top atomic layer [85]. This results in the creation of metal atoms protruding out of the surface and therefore in a local enhancement of the tip surface electric field [84]. This electric field is high enough to ionize and then field evaporate these protruding metal atoms. This etching process can be controlled by a careful adjustment of the applied voltage in order to maintain the apex field at the imaging threshold value. One reaches very small tip apex radii of curvature down to a single atom tip apex [86]. This surface diffusion completed by a field evaporation process is schematically illustrated in figure 17. The sequence of FIM images in figure 18 represents the tip apex evolution during the sharpening process. The decrease in the apex area and the increase in the spot size are direct indications of the tip sharpening as the FIM magnification increases [86].

Notice that when the tip radius is reduced to 1 or 2 nm, a few atomic layers (rings) appear on the FIM image. In this regime, the concept of atomic planes or poles is no longer valid and hence the conventional method of radius estimation cannot be used. In this case, the most appropriate way to evaluate the tip radius with good approximation is to build a bcc atomic model that can reproduce an atomic feature similar to the FIM image [83].

With this surface electric field assisted technique, it is possible to fabricate an ultra-clean tip apex with radii of curvature adapted to the lateral size of the nano-islands to be contacted. The advantage of the associated FIM image is that the tip apex atomic structure can be followed during the field assisted etching process. This opens the way to fabricate many identical tips having similar apex atomic structure and crystallographic orientation. This is very important since the tip apex work function depends on its crystallographic orientation. It is essential that all the tips converging toward a given nanostructure get the same contact conductance, that is the same work function. Notice that this local work function can be measured by changing the polarity of the tip bias voltage, transforming the FIM into a field emission microscope [86].

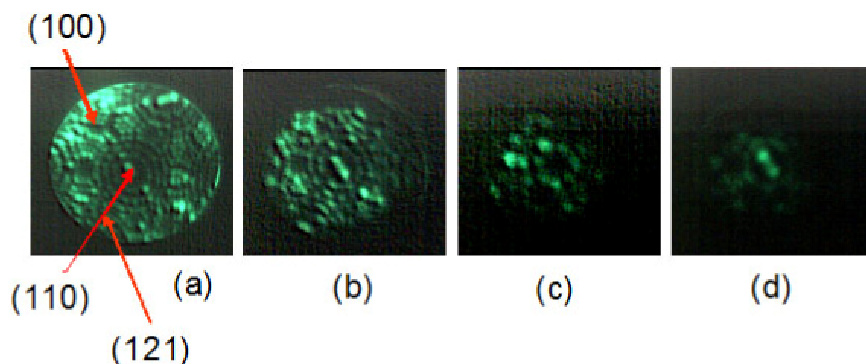

Figure 18. A sequence of FIM images following the step-by-step fabrication of a very sharp STM tip apex using the N_2 field assisted technique. (a) The initial FIM image of the tip apex with its characteristics facets. (b)–(d) a progressive increase of the electric field to reach a very sharp tip apex with only 2 W atoms at the tip apex end.

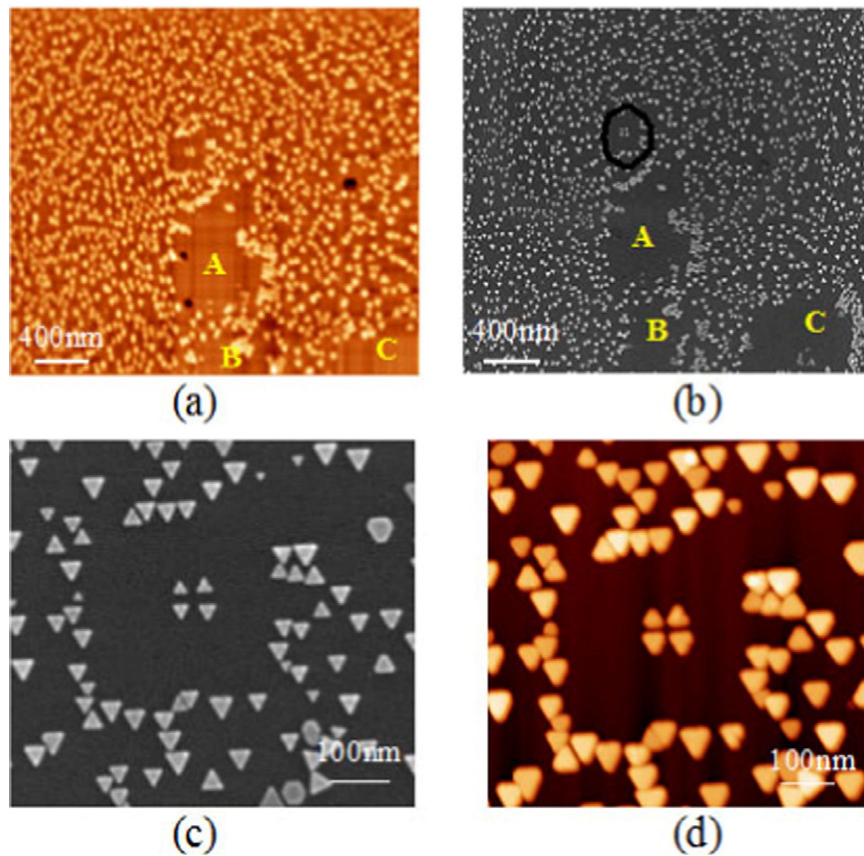

Figure 19. (a) STM image of marks A to C formed by sweeping out many Au nano-islands using the STM brushing mode, (b) SEM image of the same A to C marks after transferring the MoS_2 wafer from the UHV-STM to the SEM and searching for the A, B and C marks with a moderate SEM magnification, (c) SEM image of the nanostructure located at the mark A indicated by a black circle in (b). (d) The original STM image of the four-metallic-pad nanostructure constructed by STM manipulating single nano-islands before the transfer of the wafer from the UHV-STM to the SEM.

4.5. Navigation and the structure of the interconnection machine

The STM constructed nanostructure now exists ‘somewhere’ on the semiconductor surface. To align it with the field assisted fabricated ultra-sharp tips, described in section 4.4, a navigation system is required. It must be based on the determination of a fixed reference to pass from the nanoscale of the contacting nanostructure (∼10 nm) to the mesoscopic scale of the body of the tip (∼100 μm). Only a scanning electron microscope (SEM) is able to access such a range of scales, as indicated in figure 2(c).

Before transferring the sample from the UHV-STM to the UHV-SEM chamber and to ease the navigation on the wafer surface, the addition of appropriate marks is necessary to re-locate the contacting nanostructure over the millimeter wafer size now positioned under the UHV-SEM. This marking is performed with the STM just after the construction of the contacting nanostructure. These marks can be a simple bar code formed by brushing out many nano-islands of the semiconductor surface with a series of micronscale squares. It was also proposed to crash the UHV-STM tip, after the nano-island manipulation, near the constructed interconnection nanostructure. Whatever the marking technique, these marks must be easily imaged in a medium range magnification UHV-SEM [71].

Figure 19(a) displays the STM images of 3 marks (A, B and C) fabricated after the construction of a four metallic nanopad nanostructure. The lateral size of the marks is close to the maximum scanning ability of a standard UHV-STM but can be imaged with low SEM magnification. After transferring the sample to the UHV-SEM, these A, B and C patterns are first located on the wafer surface by the UHV-SEM (figure 19(b)). Navigating from the marks, the contacting nanostructure can be easily located in absolute direction and distance. The UHV-SEM image of the corresponding nanostructure is presented in figure 19(c), where all nano-islands are found in the same position as in the initial UHV-STM image presented in figure 19(d), recorded just before the wafer transfer from the STM to the SEM.

Following the figure 2(c) principle, the contacting machine on a semiconductor surface is made of an assembly of 3 UHV chambers. One chamber is dedicated to the wafer preparation and metallic nano-island deposition and transfer (when necessary). A second chamber is equipped with a LT-UHV-STM for fabricating the atomic wires, manipulating the molecule logic gate and positioning the metallic nano-islands, one on each termination of an atomic wire. The third chamber

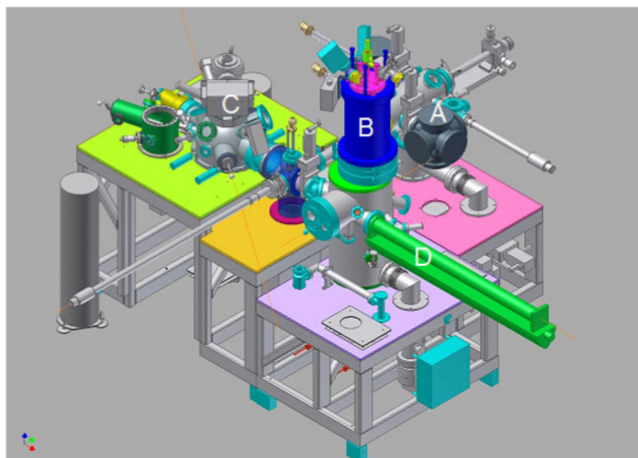

Figure 20. The final design of the IMRE (Singapore) interconnection machine with its 3 main chambers: (A) the preparation chamber with the FIM, (B) the LT-UHV-STM from Omicron Nanotechnology and (C) the nano-probe system from Omicron Nanotechnology with its UHV-SEM (3 nm resolution) and the 4 integrated STM. (D) is the LT transfer from the LT-UHV-STM to the UHV-SEM.

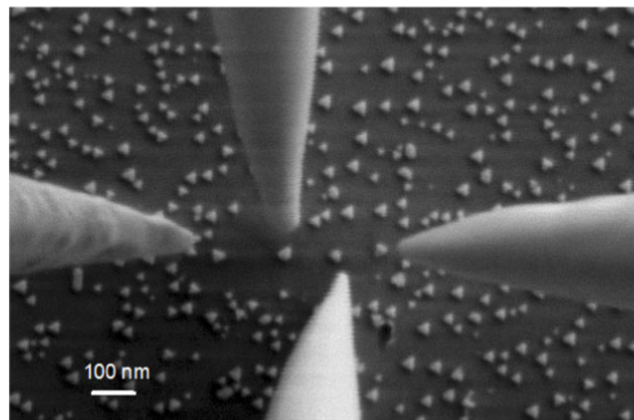

Figure 21. SEM image of the tip apex of 4 chemically etched tungsten tips converging toward 4 Au nano-islands that have been manipulated one-by-one to construct a 4 point line to perform surface conductance measurements. This image has been recorded on a multi-probe system from Zyvex.

is equipped with an UHV-SEM with a resolution better than 5 nm to be able to image the contacting metallic nano-islands and to position a tip apex on each of these nano-islands. The details of the IMRE Singapore interconnection machine are presented in figure 20.

Under the UHV-SEM, the contact between a nano-island and its tip apex is controlled by the feedback loop system of an STM to avoid the local destruction of the sample. Consequently, each tip has to be positioned on a STM mechanical system driven by its own control electronics. A SEM image of 4 nano-islands manipulated on purpose in a row on a MoS_2 surface is presented in figure 21 together where the 4 tip apices approaching for the contact. Electrical measurements are now in progress to record the 'nanopad—MoS_2 surface—nanopad' I–V characteristics for inter-nanopad distances lower than 10 nm.

5. Discussion

As presented in sections 3 and 4 of this review, it is now technically possible to construct atomic scale precision interconnection machines dedicated to contact electronically an atomic scale or a single molecule circuit as proposed in figure 2. Depending on the electronic surface gap of the supporting material, solutions have been found to navigate on the surface and to locate the active nano-area respecting the atomic precision of this surface and the atom-by-atom (or molecule-per-molecule) construction. The solutions are based on the use of two different types of microscopy at the same time: a far and a near field one. For large gap surfaces, an optical microscope is looking after a NC-AFM one. For moderate gap surfaces, an SEM is looking after an STM one. Contacting the atomic scale structure relies on the same strategy for the two types of surfaces: bridging and positioning metallic nano-islands on the surface. These nanopads are contacted using a specific nanostencil technique on large gap surfaces or multiple STM tips landing from the top of the surface on low gap surfaces. What remains to be tested is how these nanopads interact with the surface atomic wires in charge of contacting the central molecular machinery.

One drawback of these UHV interconnection machines is that each step uses a specific UHV equipment. Therefore, the sample must travel frequently in a large UHV system from equipment to equipment. A future direction would be to reduce this traveling distance by integrating a maximum number of steps in the same UHV equipment. This improvement would also significantly simplify the navigation problem.

The future of atomic scale interconnection machines will face two very difficult technological problems: the packaging and the unavoidable increase of the number N of interconnects to increase the molecule machinery complexity. The two types of interconnection machines presented in this review are laboratory equipment. When a molecule device is constructed, interconnected and characterized in UHV, there is no way yet of carrying it intact outside the UHV chamber and in certain cases increasing the substrate temperature up to room temperature. The packaging problems carried out by atomic scale technologies is almost absent in the literature and only one patent was recently issued on this problem [87].

The number of possible interconnects converging towards a given nanoscale machinery is intimately related to packaging, since, for example, it seems to be very difficult to greatly multiply the number of ultra-sharp STM tips converging toward a nanoscale area. At the surface of an atomically mastered wafer, we do not yet know practically how many metallic interconnects N can be constructed to converge towards a nano-spot of diameter D as a function of the atomic wire width δ and for a given inter-atomic wire distance d at the interconnection point. Of course, the simple geometric answer to this question is:

$$N = \pi D(d + \delta)^{-1}.$$

Using wires with a section of a single metallic atom for the interconnects, the minimum value for δ is simply twice the van

der Waals radius of the corresponding metal atom, or simply the effective lateral expansion of a surface dangling bond that is $\delta > 0.5$ nm. If we suppose that very long atomic wires can be fabricated with the methods discussed in sections 3 and 4, the limit on N for a given D is imposed by the leakage tunneling current that can be tolerated on the surface of the wafer for the performance of the atomic or molecular circuits to be measurable. Taking a standard large gap insulating surface, a leakage current intensity lower than a fA leads to $d > 1$ nm at the interconnection side between the molecule circuit and the atomic wires for a bias voltage lower than a volt. For a low gap semiconductor surface, the fA leakage current regime will be reached for $d > 10$ nm and at a much lower bias voltage. These numbers are putting an extreme constraint on the size of the molecule (or of the atomic scale circuit) that would be accessible with N electrodes. For a very complex molecule of effective lateral size of about $D = 5$ nm, $N < 10$ on an insulator and $N < 2$ on a semiconductor surface. The number N of required interconnects is limited very much by the surface electronic characteristics and care must be taken to optimize the computing power of the molecule for a given lateral extension D.

In a standard circuit design based on the Kirchhoff laws, and aside from the fabrication and the physical limits on δ and d, there is also an important architectural consideration which fortunately limits N for a given D. Already in microelectronics, the empirical law $N = kM^p$ ($k = 2.24$ and $p = 0.5$) limits the minimum number of interconnects required on average by a designer to interconnect a microprocessor logic circuit made of a assembly of M interconnected transistors [5]. For the atomic scale, if the diameter D of the molecule is too small, there will be not enough space in the molecule or in the atomic circuit to support, in a classical circuit design, a given computing power (measured for example by the complexity of the logic gate implanted in the molecule circuit). In this case, a complex logic circuit will require a very large molecule, maybe in the $D = 10$ nm range and the number N of required interconnects will be rather limited. On the contrary, if a large computing power can be implanted in a molecule, for example by a quantum approach [13], difficulties may arise since it will be impossible to make enough N atomic wires converging towards this molecule to benefit from the full computing power of the molecule in a spatial interconnection architecture. In this case, multiplexing of the data will be required, forcing the interconnection machine to use photons and not electrons to exchange data with a single molecule. This will introduce a new range of surface science studies for dielectric or plasmonic wave guides converging at the atomic scale towards a single complex molecule.

Acknowledgments

This work has been supported by the French National Research Agency DiNaMo project n°ANR-05-PNANO-014. Partial support from the European Commission within the project PicoInside (Contract n°IST-015847) is gratefully acknowledged. The authors wish to thank the European Commission, the CNRS and A*STAR for their continuous support during the definition, the design and now the construction of atomic scale interconnection machines. We are grateful to E Dujardin, T Ondarçuhu and J S Yang for their contribution to this work.

References

[1] Rapenne G, Launay J-P and Joachim C 2006 *J. Phys.: Condens. Matter* **18** S1797
[2] Joachim C, Gimzeswki J K and Aviram A 2000 *Nature* **408** 541
[3] Wada Y 1996 *Microelectron. Eng.* **30** 375
[4] Ample F, Ami S, Joachim C, Thieman F and Rapenne G 2007 *Chem. Phys. Lett.* **434** 280
[5] Joachim C 2002 *Nanotechnology* **13** R1
[6] Stojkovic S, Joachim C, Grill L and Moresco F 2005 *Chem. Phys. Lett.* **408** 134
[7] Ramachandran G K, Hopson T J, Rawlett A M, Nagahara L A, Primak A and Linsay S M 2003 *Science* **300** 1413
[8] Itoua S, Joachim C, Rousset B and Fabre N 1992 *Nanotechnology* **3** 10
[9] Saifullah M S M, Ondarçuhu T, Koltsov D F, Joachim C and Welland M 2002 *Nanotechnology* **13** 659
[10] Cacciollati O, Joachim C, Martinez J-P and Carsenac F 2004 *Int. J. Nanosci.* **3** 233
[11] Chou S Y, Krauss P R and Renstrom P J 1996 *Science* **272** 85
[12] Thet N T, Lwin M H, Kim H H, Chandrasekhar N and Joachim C 2007 *Nanotechnology* **18** 335301
[13] Duchemin I, Renaud N and Joachim C 2008 *Chem. Phys. Lett.* **452** 269
[14] Soukiassian L, Mayne A J, Carbone M and Dujardin G 2003 *Surf. Sci.* **528** 121
[15] Lin S, Li M, Dujardin E, Girard C and Mann S 2005 *Adv. Mater.* **17** 2553
[16] Ondarçuhu T, Nicu L, Cholet S, Bergaud C, Gerdes S and Joachim C 2000 *Rev. Sci. Instrum.* **71** 2987
[17] Heinz K, Bernhardt J, Schardt J and Starke U 2004 *J. Phys.: Condens. Matter* **16** S1705
[18] Feenstraa R M, Dong Y and Lee D C 2005 *J. Vac. Sci. Technol.* B **23** 1174
[19] Schönberger U and Aryasetiawan F 1995 *Phys. Rev.* B **52** 8788–93
[20] Schintke S and Schneider W-D 2004 *J. Phys.: Condens. Matter* **16** R49
[21] Giessibl F J 2003 *Rev. Mod. Phys.* **75** 949
[22] Morita S, Wiesendanger R and Meyer E 2002 *Noncontact Atomic Force Microscopy* (Berlin: Springer)
[23] Zhong Q, Innis D, Kjoller K and Ellings V B 1993 *Surf. Sci.* **290** L688
[24] Albrecht T R, Grutter P, Horne H K and Rugar D 1991 *J. Appl. Phys.* **69** 668
[25] Giessibl F J 1995 *Science* **267** 68
[26] Kitamura S and Iwatsuki M 1995 *Japan. J. Appl. Phys.* 2 **34** L145
[27] Fukuma T, Higgins M J and Jarvis S P 2007 *Phys. Rev. Lett.* **98** 106101
[28] Venegas de la Cerda M A, Abad J, Madgavkar A, Martrou D and Gauthier S 2008 *Nanotechnology* **19** 045503
[29] Bammerlin M, Lüthi R, Meyer E, Baratoff A, Lü J, Guggisberg M, Loppacher C, Gerber C and Güntherodt H-J 1998 *Appl. Phys.* A **66** S293
[30] Barth C and Henry C R 2003 *Phys. Rev. Lett.* **91** 196102
[31] Barth C and Reichling M 2001 *Nature* **414** 54
[32] Barth C, Foster A S, Reichling M and Shluger A L 2001 *J. Phys.: Condens. Matter* **13** 2061
[33] Pfeiffer 0, Gnecco E, Zimmerli L, Maier S, Meyer E, Nony L, Bennewitz R, Diedrich F, Fang H and Bonifazi D 2005 *J. Phys.: Conf. Ser.* **19** 166

[34] Bennewitz R 2006 *J. Phys.: Condens. Matter* **18** R417
[35] Nony L, Gnecco E, Baratoff A, Alkauskas A, Bennewitz R, Pfeiffer O, Maier S, Wetzel A, Meyer E and Gerber C 2004 *Nano Lett.* **11** 2185–9
[36] Burke S A, Ji W, Mativetsky J M, Topple J M, Fostner S, Gao H-J, Guo H and Grütter P 2008 *Phys. Rev. Lett.* **100** 186104
[37] Dienel T, Loppacher C, Mannsfeld S C B, Forker R and Fritz T 2008 *Adv. Mater.* **20** 959
[38] Fendrich M and Kunstmann T 2007 *Appl. Phys. Lett.* **91** 023101
[39] Trevethan T, Kantorovich L N, Polesel-Maris J, Gauthier S and Shluger A L 2007 *Phys. Rev.* B **76** 085414
[40] Bouju X, Joachim C and Girard C 1994 *Phys. Rev.* B **50** 7893
[41] Sushko M L, Gal A Y, Watkins M and Shluger A L 2006 *Nanotechnology* **17** 2062
[42] Oyabu N, Custance O, Yi I, Sugawara Y and Morita S 2003 *Phys. Rev. Lett.* **90** 176102
[43] Sugimoto Y, Abe M, Hirayama S, Oyabu N, Custance O and Morita S 2005 *Nat. Mater.* **4** 156
[44] Hirth S, Ostendorf F and Reichling M 2006 *Nanotechnology* **17** S148
[45] Joachim C, Bouju X and Girard C 1993 *Atomic and Nanometer Scale Modification of Materials: Fundamentals and Applications* (*NATO ASI Series, Series E: Applied Science*) vol 239 (London: Kluwer Academic)
[46] Meyer E 2009 personal communication
[47] Gross L, Rieder K H, Moresco F, Stojkovic S, Gourdon A and Joachim C 2005 *Nat. Mater.* **4** 892
[48] Rosei F, Schunack M, Jiang P, Gourdon A, Joachim C and Besenbacher F 2002 *Science* **296** 328
[49] Baratin R and Gourdon A 2009 *Eur. J. Org. Chem.* **7** 1022
[50] Bombis C, Kalashnyk N, Xu W, Laegsgaard E, Besenbacher F and Linderoth T R 2009 *Small* **5** 2177
[51] Lafferentz L, Ample F, Yu H, Hercht S, Joachim C and Grill L 2009 *Science* **323** 1193
[52] Joachim C and Ratner M A 2005 *Proc. Natl Acad. Sci.* **102** 8801
[53] Bauer E 1958 *Z. Kristall.* **110** 372
[54] Noguera C 1996 *Physics and Chemistry at Oxide Surfaces* (Cambridge: Cambridge University Press)
[55] Pezzagna S, Vézian S, Brault J and Massies J 2008 *Appl. Phys. Lett.* **92** 233111
[56] Lüthi R, Schittler R R, Brugger J, Vettiger P, Welland M E and Gimzewski J K 1999 *Appl. Phys. Lett.* **75** 1314
[57] Zahl P, Bammerlin M, Meyer G and Schlittler R R 2005 *Rev. Sci. Instrum.* **76** 023707
[58] Egger S, Llie A, Fu T, Chongsathien J, Kang D and Welland M E 2005 *Nano Lett.* **5** 15
[59] Guo H, Martrou D, Zambelli T, Polesel-Maris J, Piednoir A, Dujardin E, Gauthier S, van den Boogaart M A F, Doeswijk L M and Brugger J 2007 *Appl. Phys. Lett.* **90** 093113
[60] Guo H, Martrou D, Zambelli T, Dujardin E and Gauthier S 2008 *Rev. Sci. Instrum.* **79** 103904
[61] Kolbel M, Tjerkstra R W, Brugger J, van Rijn C J M, Nijdam W, Huskens J and Reinhoudt D N 2002 *Nano Lett.* **2** 1339
[62] Yan X M, Contreras A M, Koebel M M, Liddle J A and Somorjai G A 2005 *Nano Lett.* **5** 1129
[63] Kölbel M, Tjerkstra R W, Kim G, Brugger J, van Rijn C J M, Nijdam W, Huskens J and Reinhoudt D N 2003 *Adv. Funct. Mater.* **13** 219
[64] Tun T N, Lwin M H T, Kim H H, Chandrasekhar N and Joachim C 2007 *Nanotechnology* **18** 335301
[65] Vazquez-Mena O, Villanueva G, van den Boogaart M A F, Savu V and Brugger J 2008 *Microelectron. Eng.* **85** 1237
[66] Coutrot A-L, Roblin C, Lafosse X, David C, Madouri A, Laloo R and Martrou D 2009 *Microelectron. Eng.* **86** 119
[67] Akremi A, Lacharme P and Sébenne A 1997 *Surf. Sci.* **192** 377
[68] Bellec A, Riedel D, Dujardin G, Rompotis N and Kantorovich L 2008 *Phys. Rev.* B **78** 165302
[69] Hofer W A, Fisher A J, Lopinski G P and Wolkow R A 2001 *Phys. Rev.* B **63** 085314
[70] Bolland J J 1991 *Phys. Rev.* B **44** 1383
[71] Yang J S, Deng J, Chandrasekhar N and Joachim C 2007 *J. Vac. Sci. Technol.* **25** 1694
[72] Yong K S, Oltavaro D M, Duchemin I, Saeys M and Joachim C 2008 *Phys. Rev.* B **77** 205429
[73] Kiwari R K, Yang J S, Saeys M and Joachim C 2008 *Surf. Sci.* **602** 2628
[74] Hosoki S, Hosaka S and Hasegawa T 1992 *Appl. Surf. Sci.* **60/61** 643
[75] Bellec A, Ample F, Riedel D, Dujardin G and Joachim C 2009 *Nano Lett.* **9** 144
[76] Villagomez C, Zambelli T, Gauthier S, Gourdon A, Barthes C, Stojkovic S and Joachim C 2007 *Chem. Phys. Lett.* **450** 107
[77] Doumergue P, Pizzagalli L, Joachim C, Altibelli A and Baratoff A 1999 *Phys. Rev.* B **59** 15910
[78] Huang D H, Uchida H and Aono M 1992 *Japan. J. Appl. Phys.* **31** 4501
[79] Lyding J W, Chen J C, Hubacek J S, Tucker J R and Abeln C C 1994 *Appl. Phys. Lett.* **64** 2010
[80] Tanaka M, Chu F, Shimojo M, Takegushi M, Mitsuishi K and Furuya K 2006 *J. Mater. Sci.* **41** 2667
[81] Deng J, Troadec C, Kim H H and Joachim C 2009 *Nanotechnology* submitted
[82] Muller E W and Tsong T T 1969 *Field Ion Microscopy: Principles and Applications* (New York: Elsevier)
[83] Rezeq M, Joachim C and Chandrasekhar N 2009 *Microelectron. Eng.* **86** 996
[84] Rezeq M, Pitters J and Wolkow R 2007 *J. Scanning Probe Microsc.* **2** 1
[85] Rezeq M, Pitters J and Wolkow R 2006 *J. Chem. Phys.* **124** 204716
[86] Rezeq M, Joachim C and Chandrasekhar N 2009 *Surf. Sci.* **603** 697
[87] Thet N T, Joachim C and Chandrasekhar N 2009 *Patent* No WO 2009/022982 19 Feburary, Int. Patent classification: H01L 21/768 (2006.01) B82B 3/00 (2006.01)
[88] Mei W N, Boyer L L, Ossowski M M and Stokes H T 2000 *Phys. Rev.* B **61** 11425
[89] Roessler D M and Walker W C 1967 *Phys. Rev.* **159** 733–8
[90] French R H 1990 *J. Am. Ceram. Soc.* **73** 477
[91] Rubloff G W 1972 *Phys. Rev.* B **5** 662
[92] Cimalla V, Pezoldt J and Ambacher O 2007 *J. Phys. D: Appl. Phys.* **40** 6386